Second International Symposium on Marine Propulsors
smp'11, Hamburg, Germany, June 2011

A Study on Propeller Noise Emission with Special Attention to the Influence of an Ice Coverage and Finite Water Depth

Heinrich Streckwall[1], Herbert Bretschneider[1]

[1]Hamburg Ship Model Basin (HSVA), Hamburg, Germany

ABSTRACT

In the current paper, we are addressing the far field propeller pressure signal, having the 'comfort' of the ocean fauna in mind. The focus is on the combination of different boundaries limiting the water domain; namely, a free water surface, an ice cover and a sea bottom. Establishing different scenarios, we are interested in principal differences for the decay of the pressure signal. We have concentrated on the 0-100 Hz range, assuming that for that frequency range and given the task to perform a comparative study, we could neglect the finite speed of sound in water. We applied a potential based boundary element (BEM) method and derived the pressure via an approximation in the Bernoulli equation. For the merchant ship, we used an LNG hull and we concentrated on ice cover effects as we examined basically the condition where the LNG passes an open water channel surrounded by an ice covered area. Shallow water scenarios were included. A reference set up was always investigated, whereby the ice cover was completely replaced by a free water surface.

Keywords

Propeller noise, BEM, Ice cover

1 INTRODUCTION

Due to the rotating propeller, the pressure on the hull of a merchant or passenger ship has an unsteady component, which can cause vibration and noise, registered, for instance, in the accommodation for passengers or crew. The hull is just one of the boundaries surrounding the propeller, other boundaries being the free water surface and the sea ground. Until recently, only the propeller induced hull excitations were of concern in a merchant ship design process. In experiments and calculations, the propeller pressure field was thus just traced up to a few propeller diameters away from the propeller location. Far away, though, signals will decay with increasing distance; the ocean fauna will also register the working propeller, especially if considerable propeller cavitation occurs.

The radiated pressures in the frequency range from 0-100 Hz will be dominated by unsteady cavitation effects. For this frequency range, a water domain limited by a free surface (the usual case) is known to have a favorable influence on the suppression of noise radiated from the propeller. A comparably worse (however artificial) case is given by a propeller working in a flow domain which is unlimited in any direction. In view of an apparently strong effect on noise transmission imposed by the adjacent boundaries, the question arises as how a nearby ice cover would influence the noise levels.

Given the task to provide a quantitative ranking for the sound pressure level decay depending on the environmental circumstances, we replaced the cavitating propeller by a fluctuating point source of fixed amplitude and constant period for volume variation.

2 NUMERICAL APPROACH

2.1 Potential Based Formulation

We applied a potential based boundary element (BEM) method, assuming an incompressible medium whereby the hull, the ice cover, the open water and the ground entered as outer boundaries. The direct solution was given in terms of the flow potential ϕ. We derived the pressure via an approximation in the Bernoulli equation. The decisive effect of propeller cavitation was represented by a point source and the pressure field due to this source was picked up in lateral direction for points of different submergence. The source strength was chosen to produce reasonable pressure amplitudes at the hull.

As mentioned above our numerical method is based on the assumption of infinite speed of sound in water. It was tailored to the propeller hull interaction problem with special attention to cavitation (Streckwall 2003). Similar

approaches covering the treatment of the propeller have been published before by Lee (1987), Kinnas & Fine (Kinnas 1992), Kim & Lee (Kim 1996) and Streckwall (1998). As we skipped the propeller analysis for the present investigation, we just applied the module for the investigation of the hull response.

The basic quantity used to describe this problem in the framework of potential theory is the flow potential:

$$\phi_u(\vec{r},t) \tag{1}$$

which describes the unsteady part of a total potential with mean value $\phi_s(\vec{r})$. We work with the Laplace equation:

$$\nabla^2\phi_u(\vec{r},t)=0 \tag{2}$$

and thus define our added flow field as irrotational and incompressible. Principally, we derive the velocity field via $\vec{v}=-\vec{\nabla}[\phi_s(\vec{r})+\phi_u(\vec{r},t)]$, though it turns out that the velocity field (describing the rate of displacement of the fluid elements) is not essential for the unsteady pressure part $p_u(\vec{r},t)$. The latter, a disturbance to be superimposed to any steady (but irrelevant) contribution, is derived from the unsteady Bernoulli equation (valid at any arbitrary point of a streamline):

$$-\rho\partial\phi(\vec{r},t)/\partial t$$
$$+1/2\rho v^2+\rho gz+p_s(r)+p_u(r,t)=f(t) \tag{3}$$

where

- the function $f(t)$ depends only on time and not on position in the fluid,
- g is the acceleration due to gravity
- z is the elevation of the point above a reference plane

Due to a dimensional analysis based on a fluctuating point source field, we drop the $1/2\rho v^2$-term for $p_u(\vec{r},t)$ as announced above. We neglect ρgz, formally emerging due to the vertical displacement of a streamline. This means that a decomposition,

$$\phi_u(\vec{r},t)=\varphi_u(\vec{r})\cdot g(t) \tag{4}$$

would lead to the following disintegration of the fluctuating pressure:

$$p_u(\vec{r},t)=-\rho\varphi_u(\vec{r})\cdot d/dt\ \ g(t) \tag{5}$$

Setting $g(t)=\sin(kZ\omega t)$ (thus assuming a harmonic fluctuation with the k-th blade frequency knZ as $\omega=2\pi n$ with n as shaft frequency) we have:

$$p_u(\vec{r},t)=-\rho\ \varphi_u(\vec{r})\cdot kZ\omega\cos(kZ\omega t) \tag{6}$$

and we find that the factor $\varphi_u(\vec{r})kZ\omega$ is giving the pressure amplitude leaving the task to determine $\varphi_u(\vec{r})$ in 3D space in dependence of the specific boundary conditions.

In our approach, most of the boundaries (exception: free surface) are modeled via an appropriate panel system. So we represent the hull and the ice cover by panels p^1, p^2 etc. with related potentials φ_u^1, φ_u^2 etc. representing the panel loadings.

Using the flow potential φ_u^b linked to the boundary panel b as unknown, we derive a system of linear equations from self induction and mutual induction:

$$SI^b\varphi_u^b=4\pi\varphi_u^\infty+\sum\nolimits_{b'}\varphi_u^{b'}\Omega^{bb'} \tag{7}$$

where

- φ_u^∞ denotes the space function of the fluctuating point source potential
- $\Omega^{bb'}$ is the solid angle under which the boundary panel related to point b' is seen from point b (representing the mutual induction)
- SI^b = self-influence function of panel at point b

2.2 Modeling of the hull

The hull requires a panel system to be referenced as a boundary in the general flow problem. For the hull, we assume a perfectly rigid surface with 100% sound reflection characteristic. The hull panel system is confined to the aftbody part of the ship. The actual hull represents a standard LNG shape.

2.3 Modeling of the propeller

The point source was located in the propeller plane (x_o=-1.0R) showing a lateral position of y_o=0 and a vertical position of z_o=0.8 R above the propeller shaft. The volume source $\dot{V}_o$ (Volume/Time) to be positioned at (x_o, y_o, z_o) was normalized giving:

$$\dot{V}_o'=\dot{V}_o/(\omega R^3)$$

with ω denoting $2\pi n$ (n=shaft frequency), R representing the propeller radius). In the current study, it was set to $\dot{V}_o'=0.002$. When this is converted to a source strength amplitude, we provide a harmonic source fluctuating with blade rate (=nZ, Z denotes blade number) or k-th blade rate (=knZ) of $\dot{V}_o'\cos(kZ\omega t)$. $\dot{V}_o'=0.002$ gives rise to a hull pressure amplitude at blade frequency of max. 4.0 kPa in full scale, assuming a typical propeller diameter $D\cong 9.0$ m, a typical propeller revolution rate $n\cong 1.25$ Hz and a blade number of Z=6.

2.4 Treatment of Free Surface and Other Boundaries

Since water was limited on top at least partly by a free surface, we introduced a complete system of negative images reflecting the point source and all boundaries present, as well as, among these, panels representing an ice/water interface. This enforces a vanishing $\varphi_u(\vec{r})$ in the symmetry plane and according to Eq. (6) ensures a vanishing fluctuating pressure part $p_u(\vec{r},t)$. The image method is illustrated in **Figure 1**.

We set the self-influence function for hull panels to $SI^{hull}=2\pi$, for ground panels to the same value $SI^{ground}=2\pi$ and for ice panels to $SI^{ice}=2\pi$ (equivalent to a treatment of ice as a rigid cover) and to $SI^{ice}=\infty$ (enforcing $\varphi_u(\vec{r})=0$ which was equivalent to treat an ice cover as being undistinguishable from a free surface).

2.5 Principle Limitations

As noted above, we had a numerical tool right and hand that serves to investigate the hull excitation problem caused by the working propeller. If we remain on the ships aftbody or close to it, the speed of sound in water is high enough to assume that any reaction of the flow to disturbances introduced by the working propeller will happen in phase. If some cavity on the propeller expands and shrinks, the surrounding flow will immediately show a tendency to react. 'Immediately' means that the reaction time t_r is much smaller than the period of the volume fluctuation T .

If we assume 10 Hz (T =0.1s) for the fluctuating cavity, which is a typical value for the 1st blade frequency of large propellers, we may introduce a threshold of t_r >0.025s for the validity of the $t_r << T$ -assumption. With the speed of sound set to c=1480 m/s, we can estimate the size of the 'quasi-immediate' reacting fluid environment. One obtains 37m, which is ¼ of the wavelength related to 10Hz, namely λ = 148 m.

2.6 The Rigorous Approach

In the present study, we are evaluating the pressure up to about one ship length's distance from the noise source. As was shown above, our dominant frequencies are such that we will successively lose the true structure of the pressure field when going beyond some 37 m from the propeller. To resolve the complete nature of the pressure beyond 37m, the solution of the Helmholtz equation would be required. The Helmholtz equation includes effects that are dedicated to the finite speed of sound. The argument to further use the existing tool for distances beyond 37 m is based on the interpretation of **Figure 2** below. **Figure 2** introduces a hypothetic alternative to the current ground model (**Figure 1**). The total system of point sources is then asymmetrical with respect to the free surface and symmetrical in relation to the ground, reflecting the boundary conditions to be fulfilled on either surface ($\varphi_u(\vec{r}) = 0$ respectively $\partial / \partial n \varphi_u(\vec{r})$ =0).

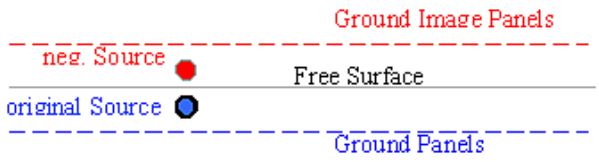

Figure 1: Current approach for the simulation of shallow water conditions in principle (omitting the hull panel system): every singularity or boundary shows a negative image above the free surface.

Figure 2 illustrates a rigorous image method, neglecting the hull and the ice cover. In this manner we address the effect of shallow water (under a free surface) principally. For simplicity, the point source was set midway between a free surface and the ground. The point sources will contribute to the pressure by a similar magnitude but alternating sign (here indicated by red and blue color). As a result the pressure sensor will show very low values, if all the signals from any source arrive without delay.

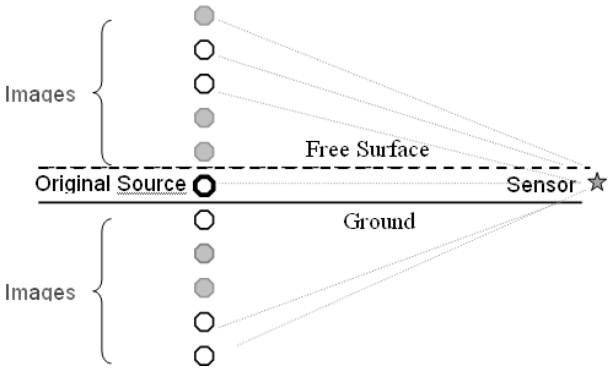

Figure 2: Shallow water effect for a point source midway between a free surface and the ground simulated solely by images. A lot of images (both signs) are required to set the boundary conditions correctly. If a pressure sensor is placed at some distance from the source-line, the point sources will contribute to the pressure by a similar magnitude but alternating sign (indicated by white and gray filling).

Figure 2 may be referenced to argue that our current method, though not providing a phase accurate superposition of pressure fields from the image chain, is still giving the correct pressures at the free surface ($\varphi_u(\vec{r}) = 0$ assured), and that realistic pressures at the ground provided the horizontal distance d_h of the sensor is reasonably larger than the water depth d_g , which should be smaller than or of order of $\lambda / 2$. Therefore, the results should be of relevance - at least for a comparison of scenarios - in between these limits with increasing significance if one approaches the water surface.

3 RESULTS

3.1 Sound Pressure Level

To be in line with the standard acoustic interpretation of noise, we provide plots of L , the Sound Pressure Level. L is a logarithmic measure of the pressure of sound relative to a reference value and is measured in decibels (dB). In particular, we used:

$$L = 20 \log (\delta p / p_{ref}) \text{ dB} \qquad (8)$$

where pref $=10^{-6}$ Pa =reference sound pressure and δp =local pressure amplitude due to source with harmonic fluctuation at 1st blade frequency. Due to the logarithmic representation of the pressure amplitudes, a plot of L vs the distance from the sound source can trace local amplitudes over several orders of magnitude.

The basic result completely describing the flow field characteristics is the velocity potential of the boundary panels (hull-, ground- and ice-panels). This gives a singularity system in terms of singularity positions and

singularity strengths that allows evaluating flow details at any location inside the water.

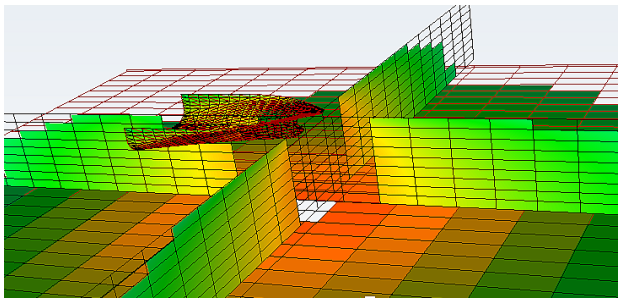

Figure 3: A grid representing hull and ground (at moderate depth=50m). An ice cover would be represented by a top-grid, omitted here to highlight the sensor system. The system of sensors is divided into 2 wire-frames, one longitudinal, one lateral. The vertical spacing of sensors is 1.0R, the horizontal spacing is 4.0 R. In some following figures the sensor points serve to built up graphs for the sound pressure level L. All graphs following below relate to x=0 and run over y (in lateral direction).

3.2 Sensors

To have access to the pressure inside the flow (off the boundaries), we used a system of probes or sensors where we evaluated the combined action of the singularities in terms of pressure amplitudes. These amplitudes were then converted to sound pressure levels L. **Figure 3** shows a typical panel system for hull and ground (at moderate depth=50m). In addition, the 2 arrays of sensor points are displayed by wire-frames. The lateral directed sensor plane runs through x=0. The longitudinal plane ranges at y=0. For both planes, the vertical spacing dz of sensors is 1.0 R and the horizontal spacing is 4.0 R. The sensor arrays have each a horizontal extent of about 225 m.

3.3 Scenarios

We start with a shallow water condition and include the ice cover on Stb (one breadth away from midship) and assume open water on port. It turned out that this setup reproduces the ice-channel –results on Stb, while on Port it duplicates the outcome for unlimited open water. We concentrate on the lateral direction. A contour plot for the sound pressure level L is given in **Figure 4**. It displays L in lateral (y-) direction, in longitudinal direction and on the ground with the aftbody of the hull partly visible. **Figure 5** shows sound pressure level curves for the lateral plane, whereby curves are distinguished by the submergence of the pressure sensor. The depth increment for the curves is 1.0R, i.e., one propeller radius. The lateral sensor points reach up to 50 propeller radii (about 225m). On the (open) port side, we recognize a strong decay of the predicted sound pressure level, covering 10 orders of magnitude within 50 propeller radii. On Stb, the ice cover starts one ship breadth from midship (about 10R) and the decay runs with another slope from this point (2 orders of magnitude within 40R). As soon as the sensors are under ice (here assumed of solid wall nature), they seem to lose any 3D structure, and they just depend on the lateral coordinate. This is different on the open side, where points close to the surface clearly show the lowest levels.

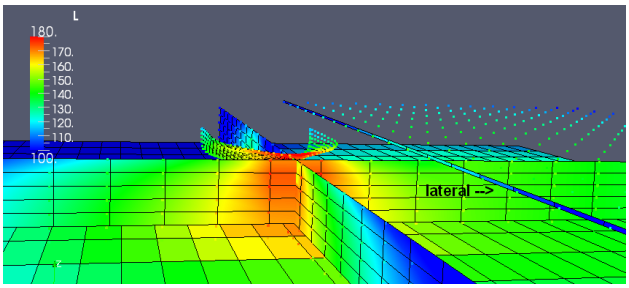

Figure 4: Shallow water, ice cover (dotted and transparent) only on Stb. The ice was given a solid wall character. Here the sound pressure levels are picked up at sensor planes x=0 and y=0 (from behind) and on the ground are given.

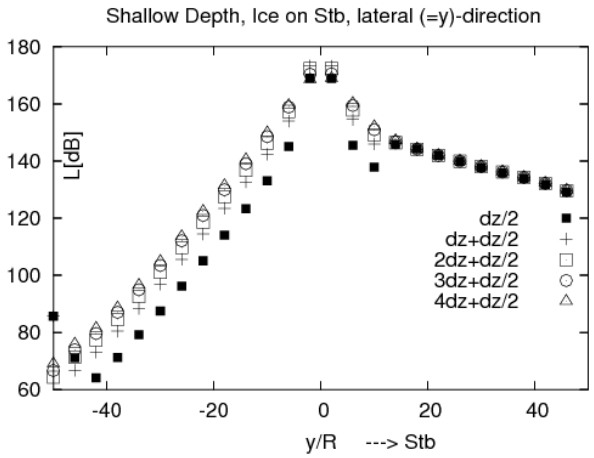

Figure 5: Transverse sound pressure levels of Figure 4 at sensor plane x=0 in graph form. Curves are indexed by the vertical sensor-distance to the water surface, where dz=1.0R.

With **Figure 6**, we changed the water depth from 30 m (shallow) to 50 m (moderate). The sound pressure levels on the open side show a reduced rate of decay, as can be read from **Figure 7**. A similar but weaker effect holds for the Stb side. Again the 3D structure on Stb is lost and no vertical decomposition of the pressure levels appears.

It might be more realistic to settle the reflection characteristics of ice somewhere between a rigid cover and a fictive boundary that allows for 100% transmission. We tried to set up such a partly transparent structure via the analogue of an adequate density of holes within an otherwise rigid cover. To allow for a certain rate of transmission of motion through the ice/water interface we changed the self-influence function SI^{ice} entering in Equation (7). Having in mind that the self-influence for a hole in the interface would be $SI^{hole} = 4\pi$ (**Figure 8**), we changed to $SI^{ice} = 2.66\pi$ for a simulation of a partly

transparent interface water/ice; further on, also called weak ice.

Figure 9 shows the results of such an attempt to change the characteristics of the ice cover into the direction of a porous structure allowing for some continuation of the incoming flow speed. That measure had a pronounced influence on the sound pressure level. The new Stb side curve is closer to the port side lines than to the Stb curve obtained previously (for rigid ice).

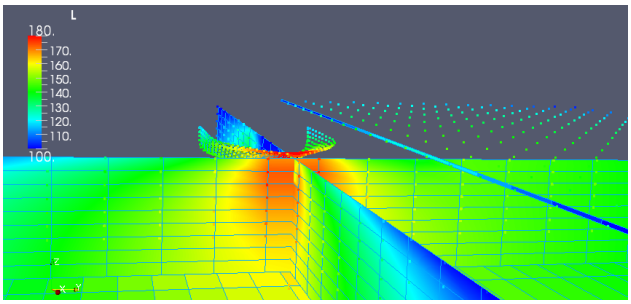

Figure 6: Medium water depth, ice cover only on Stb. The ice was given a solid wall character.

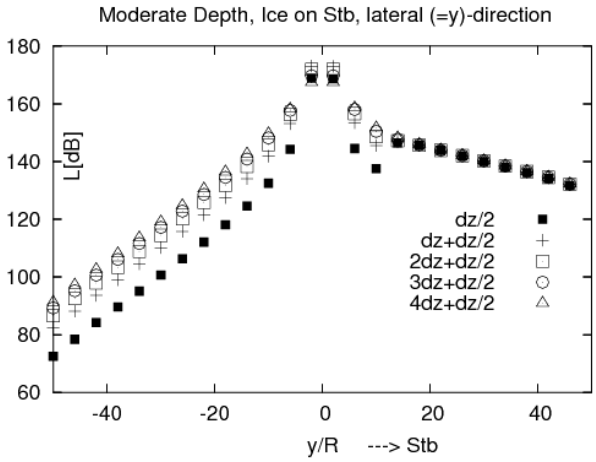

Figure 7: Transverse sound pressure levels of Figure 6 at sensor plane x=0 in graph form. The curves refer to fixed vertical sensor submergence (dz=1.0R).

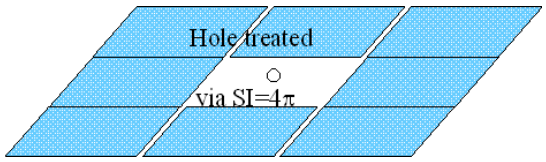

Figure 8: A hole allowing for flow through the ice cover is given $SI^{hole} = 4\pi$.

Having yet displayed solutions for scenarios with the ice confined to Stb, the graph in **Figure 10** is related to the 'channel' results, which are symmetrical to both sides and are thus plotted just for Stb. The water depth is set to infinity here. Working now with a double logarithmic scale, we included the 'limiting' curves related to unique characteristics of the upper boundary. One is related to a free surface (water against air), one denotes a free field (water against water) and one stands for a ridged surface (water against wall). The curves for the sound pressure level L are valid for a constant sensor submergence of 2.5R.

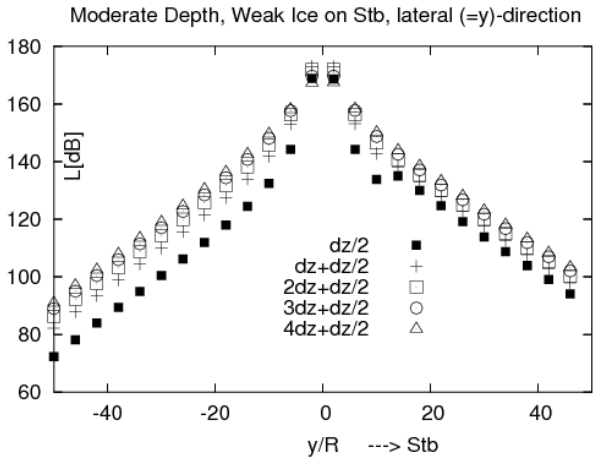

Figure 9: Changing ice characteristics for moderate depth. The curves refer to fixed vertical sensor submergence (dz=1.0R).

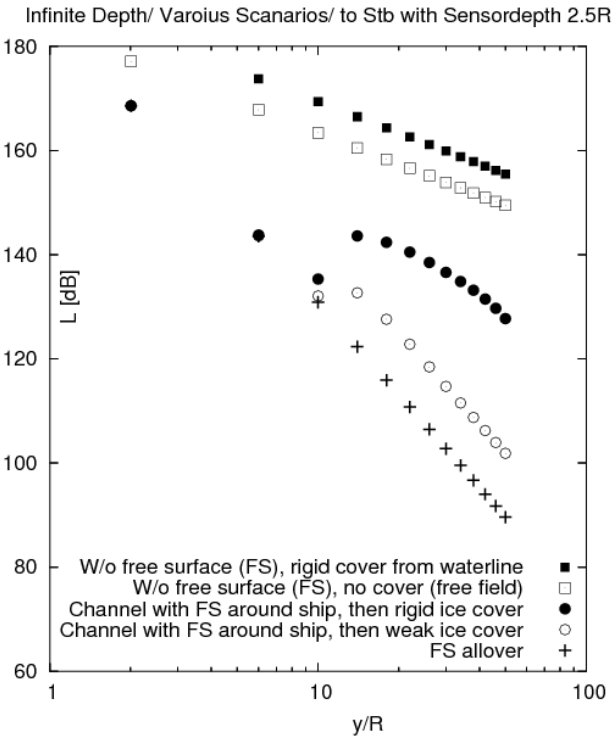

Figure 10: Sound pressure level in lateral (=y) direction at x=0 using a logarithmic length scale. One constant sensor depth z/R=-2.5; various scenarios at infinite water depth.

The reduction of pressure amplitudes caused by the presence of a partly or complete free surface environment

of the source is evident. The 'weak' ice again ranges between the two extremes, namely the rigid and the free surface model.

4 CONCLUSION

In the absence of an ice cover, a shallow water environment is favorable for the lateral and longitudinal decay of the propeller low frequency noise (8-100 Hz range). Shallow water conditions also continue to be advantageous with an ice cover present, providing there remains an open water area around the noise source (which we considered here at a depth of about one propeller radius). For shallow water, the decay of the sound pressure level seems to be a complex function of the lateral distance, which cannot be described by a single exponent.

Surrounding the open water channel by a rigid surface to simulate the ice cover effect, the sound pressure level L will rise significantly in the covered area. Replacing the free surface partly by our model for ice with a weaker reflection characteristic, L will remain close to the open water curve.

The open water area around the ships hull seems to have tremendous effects on the under ice sound pressure levels, even if water is soon (at one ship breadth aside) covered by ice. It has to be noted however, that in reality, there could be some influence from the brash ice left in an open water channel. Compared to the ideal open water way, the brash ice filled channel would tend to raise the sound pressure levels to some extent. This effect can hardly be quantified. In our model, the transmission and reflection characteristics of the ice cover represents a sensitive parameter as can be read from the alternative results, related to a free surface (water against air), to a free field (water against water) and to a ridged surface (water against wall).

We consider this study as a first step for a detailed investigation of propeller emitted noise propagation under ice. Further research is required to remove the crude approximations we are currently working with to support and to refine the current results.

ACKNOWLEDGEMENT

The results presented here characterize the basic outcome of a research project undertaken on behalf of Shell International Shipping and Trading Company (STASCO). We would like to thank STASCO for funding this kind of principle investigation, which hopefully leads the way to examine further aspects of propeller noise emission in arctic areas.

REFERENCES

Lee, J. T. (1987). Potential based panel method for the analysis of marine propellers in steady flow. PhD Thesis, Department of Ocean Engineering, MIT.

Kinnas, S. & Fine, N. (1992). 'A nonlinear boundary element method for the analysis of unsteady propeller sheet cavitation'. 19th Symposium on Naval Hydrodynamics, Seoul, Korea.

Kim, Y.-G. & Lee, C.-S. (1996). 'Prediction of unsteady performance of marine propellers with cavitation using surface-panel method'. 21st Symposium on Naval Hydrod., Trondheim, Norway.

Streckwall, H. (1998). 'Hydrodynamic analysis of three propellers using a surface panel method for steady and unsteady inflow conditions'. 22nd ITTC Propulsion Committee Propeller RANS/Panel Method Workshop, Grenoble, France.

Streckwall, H. (2003).'Numerical Models for Cavitation and Propeller Pressure Fluctuations'. Jahrbuch der Schiffbautechnischen Gesellschaft **97**, pp. 44-49.